Chinese Chemical Letters 35 (2024) 109332

Contents lists available at ScienceDirect

Chinese Chemical Letters

journal homepage: www.elsevier.com/locate/cclet

Separator functionalization enables high-performance zinc anode *via* ion-migration regulation and interfacial engineering

Ningning Zhao[a], Yuyan Liang[a], Wenjie Huo[a], Xinyan Zhu[a], Zhangxing He[a,*], Zekun Zhang[a], Youtuo Zhang[a], Xianwen Wu[b,*], Lei Dai[a], Jing Zhu[a], Ling Wang[a], Qiaobao Zhang[c,*]

[a] School of Chemical Engineering, North China University of Science and Technology, Tangshan 063009, China
[b] School of Chemistry and Chemical Engineering, Jishou University, Jishou 416000, China
[c] Department of Materials Science and Engineering, College of Materials, Xiamen University, Xiamen 361005, China

ARTICLE INFO

Article history:
Received 26 October 2023
Revised 10 November 2023
Accepted 21 November 2023
Available online 22 November 2023

Keywords:
Energy storage
Aqueous zinc ion batteries
Separators
Ion-migration regulation
Interfacial engineering

ABSTRACT

Aqueous zinc ion batteries (AZIBs) are promising energy storage devices. However, the formation of dendrites, hydrogen evolution, and corrosion reaction seriously affect their electrochemical performance. Herein, the synergistic effect of ion-migration regulation and interfacial engineering has been confirmed as the potential strategy by kaolin functionalized glass fiber separator (KL-GF) to alleviate these problems. The rapid and orderly Zn^{2+} migration was achieved to improve the transfer kinetics and induced uniform zinc deposition by more zinc-philic sites of KL-GF. Based on the interfacial engineering, the side reactions were effectively mitigated and crystal planes were regulated through KL-GF. The hydrophilicity of KL alleviated the corrosion and hydrogen evolution. Importantly, a preferential orientation of Zn (002) crystal plane by KL-GF was induced to further realize dendrite-free deposition by density functional theory (DFT) and X-ray diffraction (XRD) characterization. Hence, the Zn|KL-GF|MnO_2 cell maintained a high discharge capacity of 96.8 mAh/g at 2 A/g after 1000 cycles. This work can provide guidance enabling high-performance zinc anode for AZIBs.

Aqueous zinc ion batteries (AZIBs) have the advantages of high theoretical capacity (820 mAh/g), low redox potential, and safety [1–4]. However, zinc dendrites, hydrogen evolution reaction (HER), and corrosion reaction have seriously affected their practical applications [5–7]. For example, the uneven deposition of Zn^{2+} causes the formation of zinc dendrites, resulting in a decrease in cycle life [8]. At present, the research on the modification of zinc anode mainly focuses on the structural modification or design of electrolytes [9–11]. Compared with zinc anode and electrolyte, there are relatively few studies on separators. As an indispensable part of the cell, in addition to preventing short circuits caused by physical contact between the anode and cathode, the separator also affects the microenvironment of electrochemical reactions [12–14].

Glass fiber (GF) separators are widely used in AZIBs because of their good compatibility with aqueous electrolytes [15,16]. But the large and uneven pore size is not conducive to the orderly Zn^{2+} migration, making it easier to form zinc dendrites, leading to the damage of the GF separator [17,18]. Recently, interfacial modification plays a pivotal role in stabilizing zinc anode. The thin nonwoven paper and cotton as the separator has been reported to affect the morphology of zinc anode significantly [19,20]. The Sn coating and three dimensions (3D) metal-organic frameworks (MOFs) have been applied to the modification of separators, which are used as a deposition surface to regulate the ion-migration [21–24]. The Kaolin (KL) has potential as functionalized material [25–28]. This is attributed to its superior features including the wide source, large surface area, high specific capacitance (~ 185 F/g), excellent mechanical properties, high ionic conductivity, and abundant active sites. Notably, the structure of KL has a large number of channels and the smaller structural gap, which may accelerate the desolvation process of hydrated Zn^{2+} and provide channels for Zn^{2+}.

Herein, KL modified glass fiber separator (KL-GF) was prepared to enable high-performance zinc anode *via* ion-migration regulation and interfacial engineering (Fig. 1a). The desolvation of hydrated Zn^{2+} and uniform Zn^{2+} flux effectively inhibited the formation of by-products by the uniform-narrow aperture and chemical structure of KL-GF. Meanwhile, the rapid and orderly Zn^{2+} migration improved the transfer kinetics and induced uniform zinc

* Corresponding authors.
E-mail addresses: zxhe@ncst.edu.cn (Z. He), wxwcsu2011@163.com (X. Wu), zhangqiaobao@xmu.edu.cn (Q. Zhang).

https://doi.org/10.1016/j.cclet.2023.109332
1001-8417/

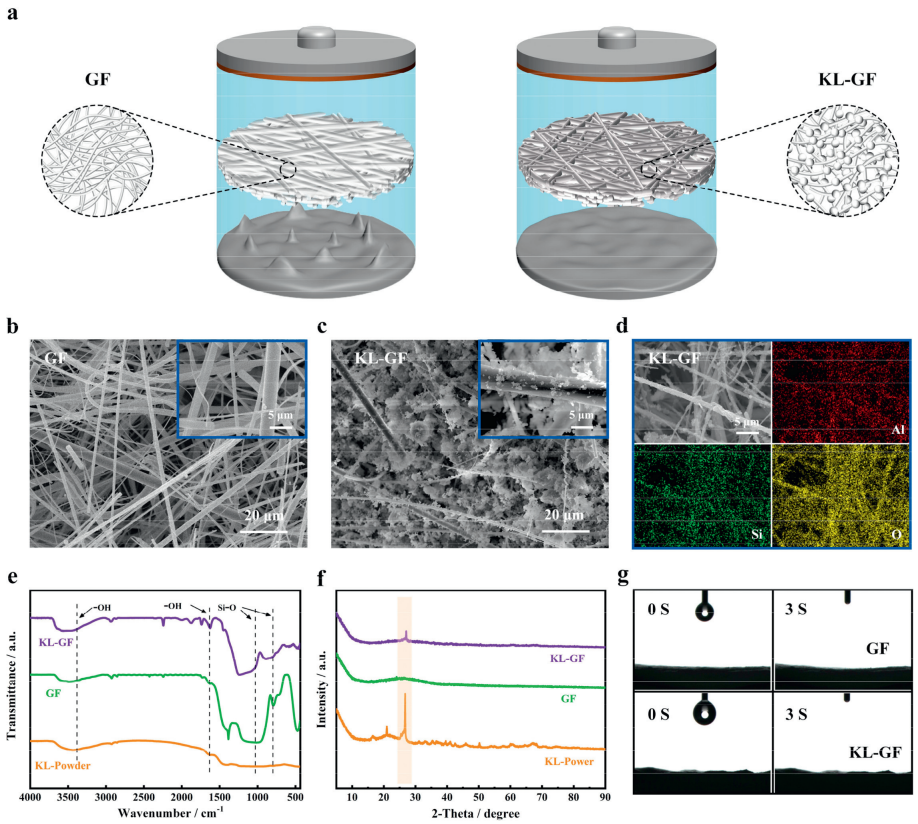

Fig. 1. (a) Model diagram of cell with GF and KL-GF, the enlarged part showing the schematic structure of the GF and KL-GF. Scanning electron microscope (SEM) images of (b) GF and (c) KL-GF at different magnifications. (d) SEM and element mapping images of KL-GF for Al, Si, and O. (e) FT-IR of KL-GF, Kaolin powder (KL-Powder) and GF. (f) XRD patterns of GF and KL-GF. (g) The wettability of GF and KL-GF after 0 s, 3 s.

deposition by more zinc-philic sites of KL-GF. Based on the interfacial engineering, the hydrophilicity of KL alleviated the occurrence of side reactions such as corrosion and hydrogen evolution. Notably, the density functional theory (DFT) showed more negative binding energy between KL and Zn (002) crystal plane, beneficial to the formation of Zn (002) crystal plane to further realize dendrite-free deposition. As a result, the Zn|KL-GF|MnO_2 cell exhibited a high discharge capacity of 96.8 mAh/g at 2 A/g after 1000 cycles. KL-GF showed great application potential in the construction of high-efficient and economical separators.

Here, KL plays a crucial role in the uniform filling effect inside GF, which provides more uniform transport channels for Zn^{2+} migration, and conducive to regulating the distribution process of Zn^{2+} and promoting the formation of uniform and smooth zinc deposition. Experimental section is shown in Supporting information. As shown in Figs. 1b and c, the uneven pore size of GF was observed, which was unconducive for the homogeneous ion-migration, and caused the formation of dendrites during the plating/stripping of the anode [29,30]. But KL has been observed to grow evenly on GF in KL-GF. At the same time, the good distribution of KL was also confirmed by its uniform element distribution (Fig. 1d, Figs. S1 and S2 in Supporting informatoin). In Fourier transform infrared spectroscopy (FT-IR) spectra, KL-GF contained the characteristic peak of KL and GF (Si-O and O-H), demonstrating that KL has also been successfully coated on GF (Fig. 1e). In X-ray diffraction (XRD) spectra, its diffraction peaks appeared at $2\theta = 27°$ was similar with KL-power, which proved the existence of KL on GF (Fig. 1f). It was worth noting that both GF and KL-GF had good wettability (0°) in Fig. 1g. Therefore, it laid an excellent experimental condition for the next experiment.

In order to estimate the effect of ion-migration regulation with KL-GF on the anode, the electrochemical performance of symmetrical and asymmetrical cells was tested. In Fig. 2a, Zn|GF|Zn cell presented a long planar diffusion with increasing current. However, Zn|KL-GF|Zn cell entered a stable 3D diffusion process after planar diffusion (14 s), which proved that Zn^{2+} was reduced to Zn^0 under the action of confined 3D diffusion, and promoted the formation of a smooth deposition layer [31,32]. This might be due to the rapid 3D diffusion and uniform growth of Zn^{2+} through the ion-confinement effect of uniform-porous structure of KL-GF. Besides, most of the KL structure gaps between atoms had smaller gaps than that of $[Zn(H_2O)_6]^{2+}$ (Figs. 2b and c). The bond angle of KL was smaller than that of the biggest bond angle for $[Zn(H_2O)_6]^{2+}$. Moreover, the diameter of Zn^{2+} (0.74 Å) was smaller than that of the KL structure gaps. Thus, the KL-GF provided a large number of channels, demonstrating that it allowed Zn^{2+} to uniformly pass and limited the passage of $[Zn(H_2O)_6]^{2+}$ [33]. In addition, the Zn^{2+} transference number with KL-GF (0.37) was larger than that of GF (0.27) in Figs. 2d and e. The abundant active sites of KL better facilitated the Zn^{2+} transport, furthermore decelerated a concentration gradient and retained good charge/discharge process [34,35]. In Figs. 2f and g, the ionic conductivity of the cell with KL-GF at 13.7 mS/cm was superior to GF at 10.1 mS/cm, but the cell with KL-GF showed a smaller resistance, which indicated the fast Zn^{2+} migration induced a lower hysteresis voltage. In Fig. 2h, the Zn|KL-GF|Cu cells had a lower nucleation overpotential of 50.6 mV than that of Zn|GF|Cu cell (62.2 mV). This suggested that the KL-GF reduced the potential barrier for zinc nucleation and facilitated homogeneous nucleation [36].

The KL-GF not only reduced the generation of zinc dendrites by regulating ion-migration, but also mitigated side reactions by regulating interfacial behavior in Fig. 3a. The corrosion current of Zn|KL-GF|Zn was lower (0.58 mA/cm^2) than that of Zn|GF|Zn (2.02 mA/cm^2) in Fig. 3b. This indicated that corrosion rate was reduced

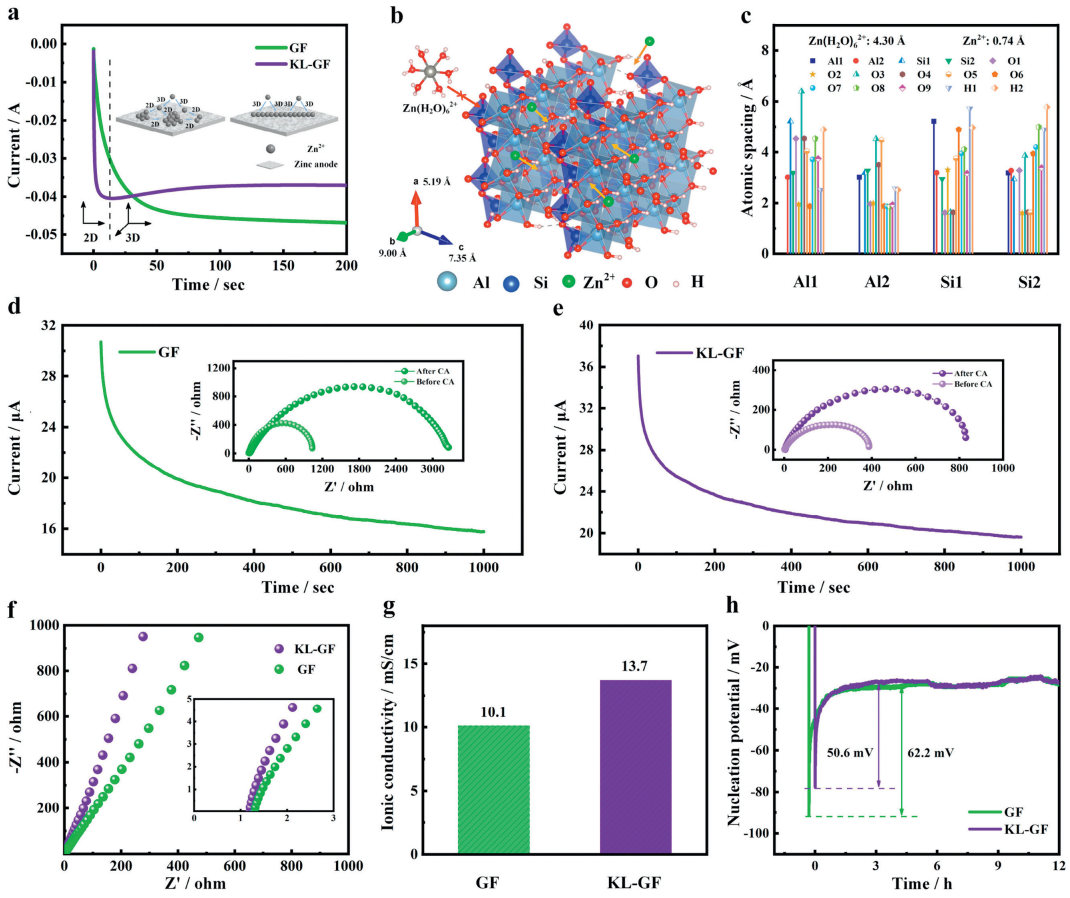

Fig. 2. (a) Chronoamperometry (CA) curve of the cells with different separators (Inset shows the 2D and 3D diffusion process of Zn^{2+}). (b) Schematic illustration of Zn^{2+} migration pathways in KL. (c) Schematic diagram of the localities and distance between atoms in KL structure. (d, e) Zn^{2+} transference number characterization of cells with different separators (Inset shows electrochemical impedance spectroscopy (EIS) spectra before and after CA). (f, g) EIS of SS|GF|SS and SS|KL-GF|SS cells for the calculation of ionic conductivity. (h) Nucleation overpotentials of Zn|GF|Cu and Zn|KL-GF|Cu cells.

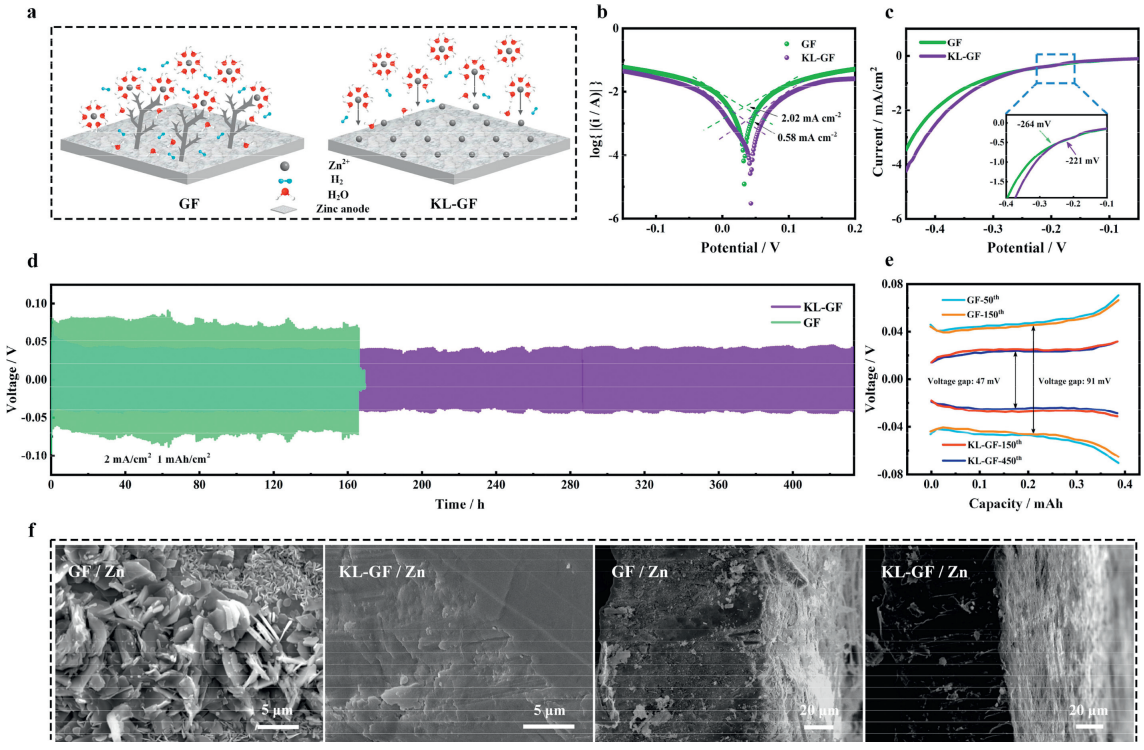

Fig. 3. (a) Schematic illustration showing a mechanism of KL-GF on zinc anode. (b) Tafel plots of Zn|GF|Zn and Zn|KL-GF|Zn cells. (c) Linear sweep voltammetry (LSV) of asymmetrical cell with GF and KL-GF separators. (d) Galvanostatic charge/discharge cycling voltage profiles of Zn|GF|Zn and Zn|KL-GF|Zn cells at current densities of 2 mA/cm^2 and 1 mAh/cm^2, respectively. (e) The voltage of gap symmetrical cells with GF and KL-GF at current densities of 2 mA/cm^2 and 1 mAh/cm^2, respectively. (f) Surface and cross-sectional SEM images of zinc anode for symmetrical cells after cycling.

to alleviate side reactions on the zinc anode by interfacial engineering [37,38]. What is more, HER potential on the cell with KL-GF (−221 mV) was higher than that of GF (−264 mV) (Fig. 3c) [39]. These were mainly due to the fact that the improved hydrophilicity of KL-GF reduced the contact between water molecules and the anode, which inhibited the corrosion reaction and hydrogen evolution. Furthermore, the stability and reversibility of enhanced cells with KL-GF were also estimated. In Figs. S3a and S4 (Supporting information), Zn|KL-GF|Zn cell (400 h) showed longer cycling stability than that of Zn|GF|Zn cell (240 h). It had better periodic stability and a lower voltage gap of 34 mV at 0.5 mA/cm^2 (Fig. S3b in Supporting information). When the current density increased to 2 mA/cm^2, the Zn|GF|Zn cell showed severe polarization (168 h). But Zn|KL-GF|Zn cell still maintained good stability (500 h) and the polarization change was smaller (Figs. 3d and e). The voltage hysteresis was lower than that of conventional cells (Fig. S5 in Supporting information), which expressed that KL-GF was beneficial to the plating/stripping process [40]. For coulombic efficiency (CE), Zn|KL-GF|Cu displayed longer cycle life (more than 200 cycles) than that of Zn|KL-GF|Cu (60 cycles) at 2 mA/cm^2 with 1 mAh/cm^2 (Fig. S6 in Supporting information). As well as the lowest overpotential at 50.33 mV was also observed, which showed that KL-GF was beneficial in improving the persistence of zinc ion plating/stripping and the reversibility of the cell. Most importantly, the surface of zinc anode in symmetrical cells with KL-GF was smoother than that of GF after cycling in Fig. 3f, indicating that it inhibited the growth of zinc dendrites and occurrence of side reactions by interfacial engineering [41].

To further investigate the synergistic effect of ion-migration regulation and interfacial engineering of the cell with KL-GF, the Zn//MnO_2 cells were assessed. The XRD and SEM of nano-fiber MnO_2 are shown in Figs. S7 and S8 (Supporting information). The shape and peak of curve were similar, which proved Zn|KL-GF|MnO_2 had good electrochemical consistency (Fig. 4a). The two sets of redox peaks showed the process of insertion and removal of Zn^{2+} and H^+ in MnO_2, respectively [42]. Charge transfer resistance

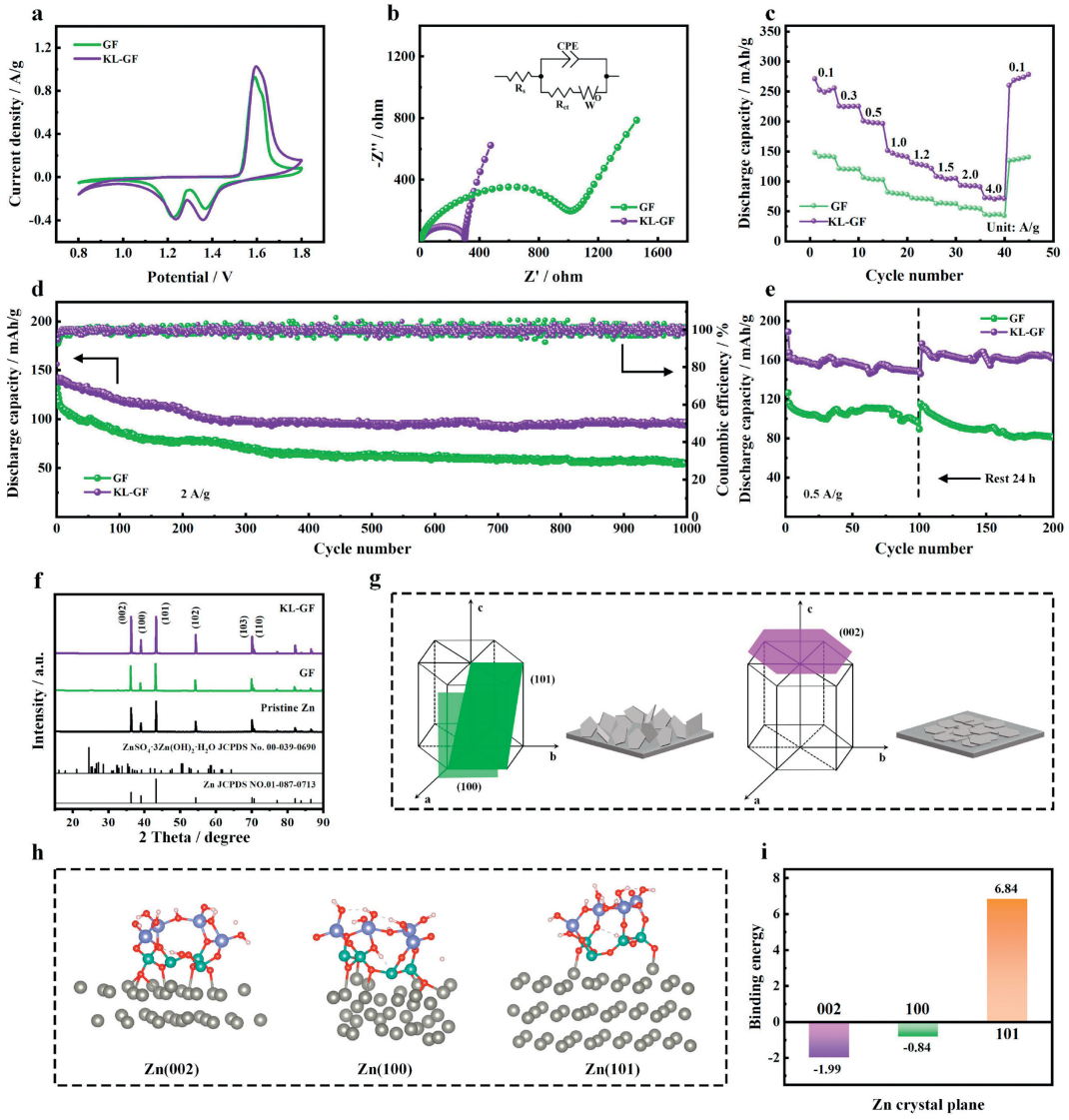

Fig. 4. (a) Cyclic voltammetry (CV) curves of Zn|GF|MnO_2 and Zn|KL-GF|MnO_2 cells. (b) EIS spectra and corresponding equivalent circuit separator of cells. (c) Rate performance of the both cells. (d) Cycling performance and CE of both cells at 2 A/g. (e) Cycling performance after resting for 24 h of both cells at 0.5 A/g. (f) XRD patterns of zinc anode for Zn|GF|MnO_2, and Zn|KL-GF|MnO_2 cells after cycling, respectively. (g) Schematic illustration of preferred orientations of Zn crystal plane. (h) Calculation models and (i) Binding energy between KL and Zn (002), (100), (101) crystal planes.

(R_{ct}) value of the cells with KL-GF (304 Ω) was lower than GF in Fig. 4b. The KL-GF reduced the charge transfer resistance, which might be beneficial to interfacial zinc nucleation [43–45]. As shown in Fig. 4c and Fig. S9 (Supporting information), the capacity of Zn|KL-GF|MnO_2 cell was always higher than that of Zn|GF|MnO_2 cell at different current densities. The cell with KL-GF could return to the initial value (0.1 A/g), indicating better reaction kinetics. Figs. S10 and S11 (Supporting information) depicted that the capacity of Zn|KL-GF|MnO_2 cell was maintained at 154 mAh/g after 500 cycles at 0.5 A/g. And the cell with KL-GF possessed high discharge capacity at 96.8 mAh/g after 1000 cycles at 2 A/g (Fig. 4d and Fig. S12 in Supporting information), indicating good stability and reversibility. This further proved the suitability of KL-GF for practical applications [46].

After cycling and resting, the discharge specific capacity of the full cell with KL-GF remained at 161.6 mAh/g, while that of the full cell with GF decreased the most significantly, reaching 81.5 mAh/g (Fig. 4e). This represented a positive contribution of KL-GF to the recovery ability of the cell after the standstill period [47]. The crystal structures on the anode after cells cycling were investigated in Figs. 4f and g. The peaks of 36.2° and 39° were related to plane Zn (002) and Zn (101), respectively. The zinc anode of Zn|KL-GF|MnO_2 cell showed extremely strong orientation of Zn (002) crystal plane. When Zn^{2+} was deposited on the Zn (002) crystal surface, a flat and uniform deposition layer was obtained. However, when Zn^{2+} was deposited on the Zn (100) and Zn (101) crystal planes, they tended to deposit in a vertical or inclined state, making it easy to generate zinc dendrites. In addition, the binding energy between KL and Zn (002), (100), (101) crystal planes were analyzed by DFT calculation in Figs. 4h and i. It revealed that the binding energy of KL and Zn (002) was more negative than that of Zn (100) and Zn (101). The theoretical results also confirmed that KL-GF could also effectively induce the horizontal deposition of Zn^{2+} along the Zn (002) crystal plane [48]. Besides, the O-2p orbital was similar to the density of states peak of Zn, indicating it had obvious orbital hybridization, which further illustrated the bonding strength between KL and Zn (002) crystal plane (Fig. S13 in Supporting information). In order to further prove the effect of KL-GF for interfacial engineering, visual data was provided in Fig. S14 (Supporting information). The anode of Zn|KL-GF|MnO_2 cell after cycling had smooth surface and dense morphology. But there are many large cracks on GF. What is more, the EDX spectra also showed that the S and O elements on Zn|KL-GF|MnO_2 cell were lower than that of Zn|KL-GF|MnO_2 cell (Fig. S15 in Supporting information). These indicated that the occurrence of side reactions and dendrites were inhibited on the zinc anode after cycling.

In summary, the KL-GF separator exerted the synergistic effect for stable zinc anode *via* ion-migration regulation and interfacial engineering. The more uniform-pore structure and chemical structure on KL-GF were beneficial to homogenize Zn^{2+} flux. A large number of channels in KL allowed Zn^{2+} to uniformly pass and limited the passage of $[Zn(H_2O)_6]^{2+}$ by ion-migration effect. The interface behavior was effectively improved through interface engineering, mitigating hydrogen evolution, corrosion, the formation of by-products and regulation of crystal planes. Importantly, DFT calculation and XRD spectra showed a preferential orientation of Zn (002) crystal plane in comparison with that of KL-GF, which made Zn^{2+} uniform deposition along the horizontal direction on the Zn (002) crystal plane, further suppressing the growth of dendrites. Therefore, Zn|KL-GF|MnO_2 cells showed excellent cycling stability and reversibility at 2 A/g after 1000 cycles. It can provide a favorable reference for the development of functionalized separators in AZIBs.

Declaration of competing interest

The authors declare that they have no known competing financial interests or personal relationships that could have appeared to influence the work reported in this paper.

Acknowledgments

This work was supported by the National Natural Science Foundation of China (Nos. 51872090, 51772097, 82204604), the Hebei Natural Science Fund for Distinguished Young Scholar (No. E2019209433), the Youth Talent Program of Hebei Provincial Education Department (No. BJ2018020), the Natural Science Foundation of Hebei Province (Nos. E2020209151, E2022209158, H2022209012). Meanwhile, we are grateful to Computing Center of Shandong Key Laboratory of Biophysics for essential support.

Supplementary materials

Supplementary material associated with this article can be found, in the online version, at doi:10.1016/j.cclet.2023.109332.

References

[1] A. Naveed, G.T. Li, A. Ali, et al., Nano Energy 107 (2023) 108175.
[2] X.R. Wang, A. Naveed, T.Y. Zeng, et al., Chem. Eng. J. 446 (2023) 137090.
[3] W.S. Gou, T. Jiang, W. Wang, et al., Chin. Chem. Lett. 34 (2023) 107760.
[4] F. Yu, Y. Wang, Y. Liu, et al., Rare Met. 41 (2022) 2230–2236.
[5] J. Wang, Y. Yang, Y. Zhang, et al., Energy Storage Mater. 35 (2021) 19–46.
[6] Y. Li, D. Zhao, J. Cheng, et al., Chem. Eng. J. 452 (2023) 139264.
[7] B.K. Wu, Y.B. Mu, Z. Li, et al., Chin. Chem. Lett. 34 (2023) 107629.
[8] P. He, J. Huang, ACS Energy Lett. 6 (2021) 1990–1995.
[9] Q.F. Li, X.X. Ye, H. Yu, et al., Chin. Chem. Lett. 33 (2022) 2663–2668.
[10] H. Qin, W. Kuang, N. Hu, et al., Adv. Funct. Mater. 32 (2022) 2206695.
[11] T.T. Wang, P.J. Wang, L. Pan, et al., Adv. Energy Mater. 13 (2022) 2203523.
[12] L.P. Zhang, X.L. Li, M.R. Yang, et al., Energy Storage Mater. 41 (2021) 522–545.
[13] P.L. Zhou, D.X. Yao, H.Q. Liang, et al., Ceram. Int. 49 (2023) 1381–1389.
[14] Y. Min, T.D. Liu, B. Zhang, et al., J. Membrane Sci. 677 (2023) 121617.
[15] H. Jia, K.Y. Liu, Y.T. Lam, et al., Adv. Fiber Mater. 5 (2022) 36–58.
[16] W. Hu, J.G. Ju, Y.X. Zhang, et al., J. Mater. Chem. A 10 (2022) 24761–24771.
[17] L.S. Wu, Y. Zhang, P. Shang, et al., J. Mater. Chem. A 9 (2021) 27408–27414.
[18] Y. Zhang, X. Li, L.S. Fan, et al., Cell Rep. Phys. Sci. 3 (2022) 100824.
[19] M.C. Liu, H.J. Chen, G. Wu, et al., Chin. Chem. Lett. 34 (2023) 107546.
[20] P.H. Cao, H.C. Zhou, X.Y. Zhou, et al., ACS Sustain. Chem. Eng. 10 (2022) 8350–8359.
[21] W. Guo, Y. Zhang, X. Tong, et al., Mater. Today Energy 20 (2021) 100675.
[22] L. Gou, J.R. Li, K. Liang, et al., Small 19 (2023) 2208233.
[23] F.F. Zhang, G.G. Wang, J. Wu, et al., Angew. Chem. Int. Ed. (2023) e20230943.
[24] Z. Peng, Y.H. Li, P.C. Ruan, et al., Coordin. Chem. Rev. 408 (2023) 215190.
[25] Y.F. Yang, G.L. Meng, H.L. Wang, et al., Chem. Eng. J. 451 (2023) 138914.
[26] H.T.T. Le, T. Dang, N.T.H. Chu, et al., Electochim. Acta 332 (2020) 135399.
[27] R. Abbas, M.A. Khereby, H.Y. Ghorab, et al., Clean Technol. Environ. Policy 22 (2020) 669–687.
[28] J. Chen, K. Zhao, L. Liu, et al., e-Polymers 22 (2022) 986–996.
[29] F.F. Wu, F.K. Du, P.C. Ruan, et al., J. Mater. Chem. A. 11 (2023) 11254–11263.
[30] Y.C. Liang, D.T. Ma, N. Zhao, et al., Adv. Funct. Mater. 32 (2022) 2112936.
[31] C.B. Deng, X.S. Xie, J.W. Han, et al., Adv. Funct. Mater. 30 (2020) 2000599.
[32] Y. Guo, W.L. Cai, Y. Lin, et al., Energy Storage Mater. 50 (2022) 580–588.
[33] K. Wu, J. Yi, X.Y. Liu, et al., Nano-Micro Lett. 13 (2021) 79.
[34] L. Hong, X.M. Wu, L.Y. Wang, et al., ACS Nano 16 (2022) 6906–6915.
[35] D. Xie, Y. Sang, D.H. Wang, et al., Angew. Chem. Int. Ed. 62 (2023) 202216934.
[36] M.H. Zhu, Q. Ran, H.H. Huang, et al., Nano-Micro Lett. 14 (2022) 219.
[37] B. Li, S.D. Liu, Y.F. Geng, et al., Adv. Funct. Mater. (2023) 2214033.
[38] H. Zhang, Z. Luo, W.T. Deng, et al., Chem. Eng. J. 461 (2023) 142105.
[39] B.Y. Tang, L.T. Shan, S.Q. Liang, et al., Energy Environ. Sci. 12 (2019) 3288–3304.
[40] P. Ye, X.W. Lei, K.D. He, et al., J. Power Sources 558 (2023) 232622.
[41] C.P. Xi, Y.B. Xiao, C.K. Yang, et al., J. Mater. Chem. A 11 (2023) 6522–6529.
[42] X.S. Wu, G.G. Liu, S.N. Yang, et al., Chin. Chem. Lett. 34 (2023) 107540.
[43] X.R. Wang, Y.L. Wang, A. Naveed, et al., Adv. Funct. Mater. (2023) 2306205.
[44] Z.X. Zhu, Z.W. Lin, Z.W. Sun, et al., Rare Met. 41 (2022) 3729–3739.
[45] C.L. Zhu, H.L. Wang, W.J. Fan, et al., Rare Met. 41 (2022) 2505–2516.
[46] H.R. Luo, J.B. Deng, Q.Z. Gou, et al., Chin. Chem. Lett. 34 (2023) 107885.
[47] M. Kim, J. Lee, Y. Kim, et al., J. Am. Chem. Soc. 145 (2023) 15776–15787.
[48] J.D. Wang, Wang R, Z.X. Liu, et al., ACS Nano 17 (2022) 1610–1621.